Please cite the Published Version

Data Access Statement: Data will be made available on request.

Title: Generation of a novel immunodeficient mouse model of Mucopolysaccharidosis type IIIA to test human stem cell-based therapies

Oriana Mandolfo[1], Helen Parker[2], Asma'u Usman[1], Yuko Ishikawa Learmonth[1], Rebecca J Holley[1], Andrew MacDonald[2], Tristan McKay[3], Brian Bigger[1, 4].

Author affiliations:

[1]Division of Cell Matrix Biology and Regenerative Medicine, Faculty of Biology, Medicine and Health, University of Manchester, 3.721 Stopford Building, Manchester M13 9PT, UK.

[2]Lydia Becker Institute of Immunology and Inflammation, School of Biological Sciences, Faculty of Biology, Medicine and Health, University of Manchester, Manchester Academic Health Science Centre, Manchester, UK.

[3]Centre for Bioscience, The Manchester Metropolitan University, E206 John Dalton Building, Manchester M1 5GD, UK.

[4]Centre for Regenerative Medicine, Institute for Regeneration and Repair, University of Edinburgh, Edinburgh BioQuarter, 5 Little France Drive EH16 4UU, Edinburgh, UK.

Abstract

Mucopolysaccharidosis Type IIIA (MPSIIIA) is a rare inherited lysosomal storage disease caused by mutations in the SGSH gene. This genetic variation results in the deficiency of the N-sulfoglucosamine sulfohydrolase enzyme, preventing the breakdown of heparan sulfate within lysosomes. The progressive accumulation of partially degraded substrate ultimately leads to brain pathology, for which there is currently no approved treatment. An established MPSIIIA mouse model has proved to be a vital asset to test several brain-targeting strategies. Nonetheless, the assessment of human stem cell-based products, an emerging research field, necessitates the use of an immunocompromised xenogeneic disease model. In the present study, we addressed this issue by generating a highly immunodeficient mouse model of MPSIIIA (NOD/SCID/GammaC chain null-MPSIIIA) through five generations of crossing an established MPSIIIA mouse model and a NOD/SCID/GammaC chain null (NSG) mouse. The immune system composition, behavioural phenotype and histopathological hallmarks of the NSG-MPSIIIA model were then evaluated. We demonstrated that NSG-MPSIIIA mice display compromised adaptive immunity, ultimately facilitating the successful engraftment of human iPSC-derived neural progenitor cells in the brain up to three months post-delivery. Furthermore, female NSG-MPSIIIA exhibit spatial working memory deficits and hyperactive behaviour, similar to MPSIIIA mice, which usually manifest around 5 months of age. NSG-MPSIIIA mice also developed primary disease-related neuropathological features in common with the MPSIIIA model, including lysosomal enlargement with storage of excess sulphated heparan sulphate and increased gliosis in several areas of the brain. In the future, the NSG-MPSIIIA mouse model holds the potential to serve as a valuable platform for evaluating human stem-cell based therapies for MPSIIIA patients.

Introduction

Mucopolysaccharidosis type IIIA (MPSIIIA), or Sanfilippo A syndrome, exemplifies a neuronopathic LSD with a compelling need for neural stem cell therapy. This genetic disorder arises from mutations in the *SGSH* gene, resulting in a deficiency of the glycosaminoglycan degrading enzyme N-sulfoglucosamine sulfohydrolase (1, 2). This ultimately leads to progressive accumulation of partially degraded heparan sulphate (HS) within the lysosome alongside widespread cellular dysfunction, particularly evident in the brain (3). Symptoms usually manifest within the first three years of age and include slowing cognitive development, which generally reveals through speech delay and loss of social and communicative skills, as well as behavioural problems, including hyperactivity and aggression (4). Current therapeutic interventions, such as enzyme replacement therapy (ERT) and allogeneic haematopoietic stem cell transplantation (HSCT), exhibit minimal efficacy in MPSIIIA patients (5), likely attributable to insufficient enzyme levels reached within the CNS. Furthermore, ongoing clinical trials based on AAV-mediated gene therapy and HSC gene therapy (HSCGT) approaches only demonstrate positive outcomes in patients treated at early disease stages (< 2 years of age), prior to the onset of significant neurodegeneration (6). Recognising the potentially irreversible neuronal damage in older patients, a regenerative approach becomes imperative. Intracranial delivery of induced pluripotent stem cells (iPSC) derivatives, particularly neural progenitor cells (NPCs), has emerged as a promising avenue, offering both functional and structural support to the brain (7).

We previously fully phenotyped and characterised a spontaneously occurring MPSIIIA mouse model (8) crossed for 10 generations onto the C57BL/6J background (9). This deliberate process aimed to minimise behavioral discrepancies, enhancing the model's reliability. This model fully recapitulated extensive HS storage and secondary accumulation of additional substrates, as well as significant neuroinflammation, seen in patients (10). This was complemented in female mice by a hyperactivity phenotype, reduced sense of danger and a working memory defect compared to the WT littermate control (9, 11). Although this model has proved to be an extremely useful tool to test the pre-clinical safety and efficacy of an HSCGT approach for both enzyme delivery and anti-inflammatory approaches (11-13), immunocompromised xenogeneic models are currently the recommended platform to test any human stem cell-based product-related toxicity and safety (14).

Despite accepting allogeneic and xenogeneic grafts, MPS mouse models employing a NOD/SCID (Non-Obese Diabetic/Severe Combined Immunodeficiency; NS) immunodeficient background still face challenges such as limited long-term engraftment of human cells and

susceptibility to thymic lymphomas (15). These limitations are addressed in NOD.Cg-*Prkdc*[scid] I[Scid] *Il2rg*[tm1Wjl]/SzJ (NSG) mice, recognised as the gold standard immunodeficient mouse strain for xenotransplantation. Notably, NSG mice lack functionally mature T-cells and B-cells, attributed to the scid mutation in the DNA repair complex protein *Prkdc*, and also exhibit impaired natural killer (NK) cell maturation due to the absence of the interleukin-2 receptor (16). This is particularly relevant, as historically, persistence of NK cells was a major barrier to the engraftment of primary human HSCs (17, 18). As a result, NSG mice are more permissive hosts for allogeneic or xenografted cells, ultimately making them a powerful platform for clinical translation of human stem cell-based products (19). In this regard, an MPSI mouse model based on an NSG background was generated by *Mendez et al.* through breeding MPSI-NOD/SCID mice with NSGs (20). This model allowed engraftment of human neural and hematopoietic stem cells up to 9 months post-injection and proved to be tumor-free.

In order to test the therapeutic efficacy and safety of iPSC-derived NPCs delivery for the treatment of MPSIIIA neuropathology, we have followed a similar approach and generated an NSG-MPSIIIA mouse model of disease. Since we believe that many groups do not develop complex immunodeficient models such as NSG/disease due to concerns over difficulties in breeding and selecting for 3 genes and a strain background change, we also aim to illustrate a methodology for breeding and characterising immunocompromised strain crosses rapidly. The NSG-MPSIIIA model recapitulated the neuropathological and behavioural features of Sanfilippo syndrome type A, while retaining the immunodeficient properties of NSG mice. This ultimately allowed successful engraftment of iPSC-derived NPCs in the brain, offering a valuable insight for prospective therapeutic interventions and presenting a pathway for the generation of multiple immunodeficient LSD models in future.

Results

Generation of the NSG-MPSIIIA mouse model

B6.Cg-*Sgsh*^{mps3a}/6J (MPSIIIA) mice were originally obtained as a naturally occurring *Sgsh* mutant (D31N) which retains 3-4% residual SGSH activity (8). These mice were backcrossed for over 10 generations to a C57Bl/6 background (9). NOD.Cg-*Prkdc*^{Scid} *Il2rg*^{tm1Wjl}/SzJ-*Sgsh*^{mps3a}/6J (NSG-MPSIIIA) mice were generated by crossing MPSIIIA (B6.Cg-*Sgsh*^{mps3a}/6J) mutant males with NOD.Cg-*Prkdc*^{Scid} *Il2rg*^{tm1Wjl}/SzJ (NSG) females. The male heterozygous offspring obtained from the first cross were backcrossed to female NSG mice to obtain second generation heterozygous MPSIIIA (Aa) offspring, also mutant for both *Prkdc* (SCID) and *Il2rg* (Common Gamma C chain) (ss and gg, respectively) and this breeding strategy was repeated until the fourth generation (*Figure 1*). To reduce inbreeding and maximize genetic variability, a proportion of the fourth generation was backcrossed to NSG mice, resulting in a fifth generation. The latter was then crossed with the remaining proportion of the fourth generation to obtain sixth generation homozygous recessive and wild-type MPSIIIA (aa and AA, respectively) offspring, also mutant for both *Prkdc* (SCID) and *Il2rg* (Common Gamma C chain) (ss and gg, respectively).
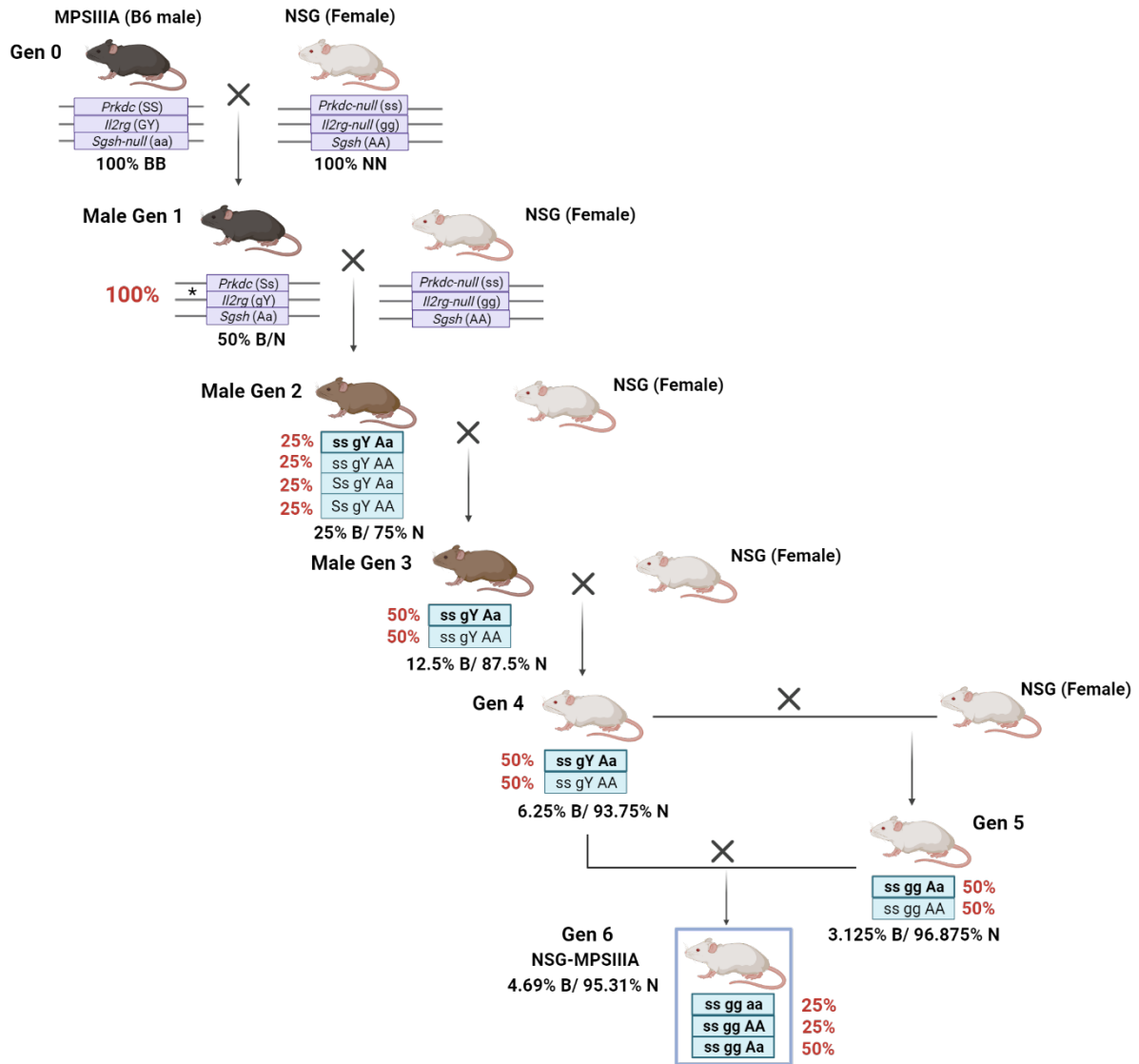
Figure 1: Generation of the NSG-MPSIIIA mouse model

A B6 MPSIIIA male was crossed to an NSG female and the selected male offspring were backcrossed to NSG females for five generations. B stands for B6 strain, while N stands for NOD strain. S/s denotes the *Prkdc* gene, G/g or gY denotes the X linked *Il2rg* gene, and A/a denotes the *Sgsh* gene. The genes symbolized as upper case are dominant while those designated by lower case are recessive. Since the *Il2rg* gene is X-linked, the males obtained in generation 1 were all mutant for this gene (denoted as *). The blue boxes with the text in bold show the genotype that was selected to cross the next MPSIIIA male with an NSG female. Fifth generation mice were crossed with a proportion of the fourth generation to obtain sixth generation homozygous recessive and wild-type MPSIIIA (aa and AA, respectively) offspring, also mutant for both *Prkdc* (scid) and *Il2rg* (Common Gamma C chain) (ss and gg, respectively).The heterozygous littermates (Aa) were used for breeding purposes. Further backcrossing onto NSG will be implemented for future studies.

The NSG-MPSIIIA mice are highly immunocompromised

In order to confirm that the NSG-MPSIIIA model recapitulates all aspects of the NSG immune system defects, we compared the immune composition between C57BL/6J (WT), NSG and NSG-MPSIIIA mice in the blood, spleen and thymus by flow-cytometry analysis (*Figure 2*). Overall, our newly generated NSG-MPSIIIA mouse model fully resembled the NSG mice regarding both innate and adaptive cellular composition. Notably, both NSG and NSG-MPSIIIA mice showed a significant deficiency of T-cells, B-cells and NK cells when compared to WTs, except for thymic NK cells, which displayed an increase instead. In this respect, there are functionally distinct populations of NK cells that specifically arise in the thymus (21), which might not be susceptible to the *Il2rg*^{null} mutation. Interestingly, an average 16- and an 18-fold increase in % of total neutrophils was detected in the blood and spleen respectively for both NSG and NSG-MPSIIIA, when compared to WT. A similar increase was also observed for both monocytes and macrophages in the spleen (*Figure 2*), despite the NSG-MPSIIIA mice displaying half as many monocytes in the blood, when compared to the NSGs.
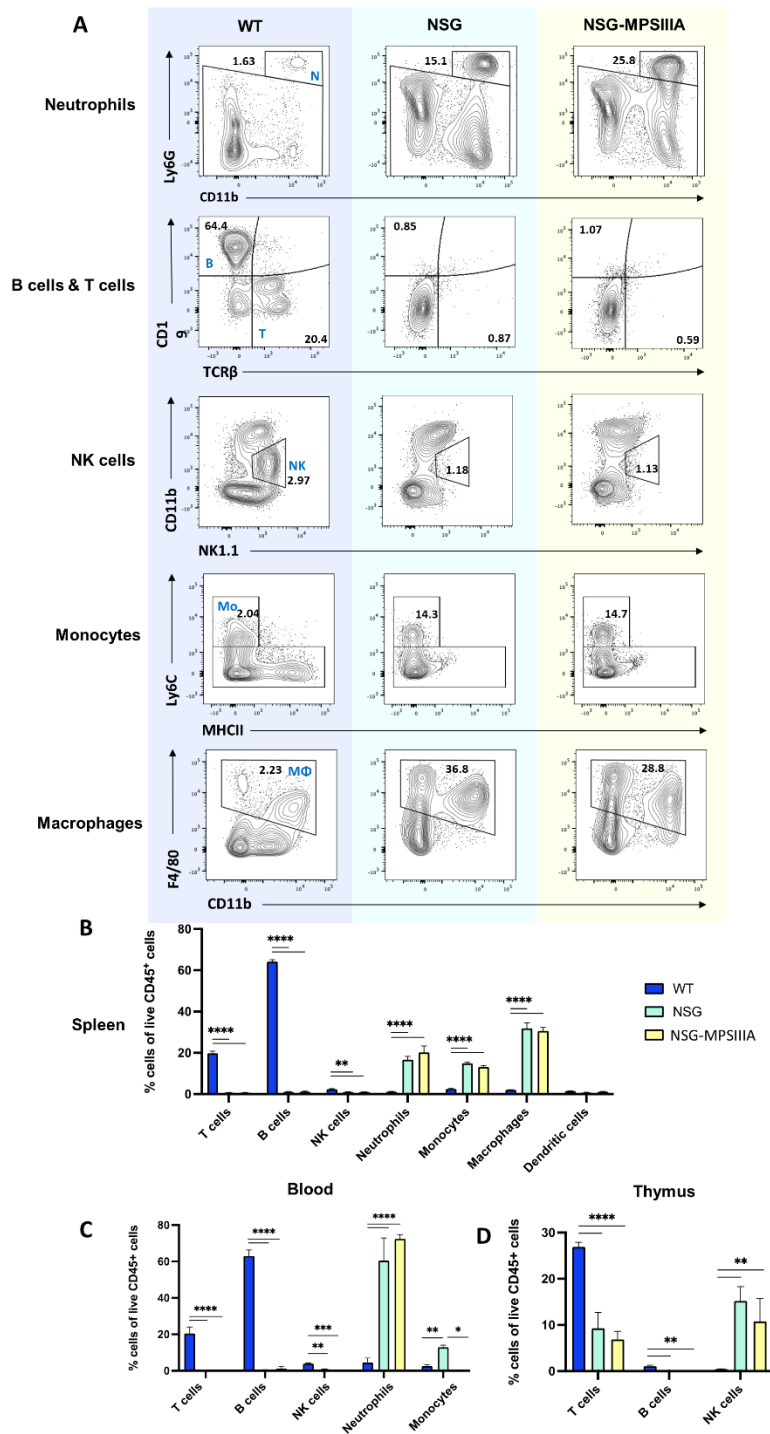
Figure 2: The NSG-MPSIIIA mice are highly immunocompromised

(**A**) Representative flow plots, with the numeric values indicating the % frequency of live CD45+ cells. % cells of live CD45+ T-cells, B-cells, NK cells, neutrophils, monocytes, macrophages and DCs in whole spleen (**B**), blood (**C**) and thymus (**D**) of 2-4-month old B6 WT, NSG and NSG-MPSIIIA animals (n= 3). The % of CD45+ cells was measured by flow cytometry and further analysed with FlowJo v10. Significant differences are determined by two-way ANOVA with Tukey's post hoc analysis, *P < 0.05, **P < 0.01, ***P < 0.001 and ****P < 0.0001. Error bars represent standard error of the mean (SEM). Comparisons between groups are shown with a line.

Female NSG-MPSIIIA mice exhibit impaired spatial working memory and hyperactivity

Once having confirmed that the NSG-MPSIIIA mouse model was highly immunocompromised, we also assessed whether this new model had retained the behavioural abnormalities that characterise the B6.Cg-*Sgsh*mps3a model (9). In this respect, both spatial working memory and hyperactive behavior were assessed through Y-maze spontaneous alternations test and open-field test, respectively, at 4 and 5 months of age. At 4 months of age, no significant differences in behaviour were observed between the two groups (*Figure 3a-c*). Only after 5 months of age, the NSG-MPSIIIA mice displayed a significant reduction (13.2%) in spatial working memory, when compared to their WT littermates (*Figure 3d*). In addition, the NSG-MPSIIIA mice also displayed a significant increase (1.4-fold) in total distance travelled and velocity, when compared to their WT littermates (*Figure 3e*). Despite not being significant, an increasing trend was also observed in mobility (where immobility is <4%, mobile is 4-10% and highly mobile is >10%) which, together with the above-mentioned parameters, suggest hyperactive behaviour in NSG-MPSIIIA mice at 5 months of age. Lastly, the NSG-MPSIIIA group displayed a tendency to spend more time in the inner zone, ultimately suggesting a reduced sense of danger in the mouse model, in line with what is observed in patients (*Figure 3e*).
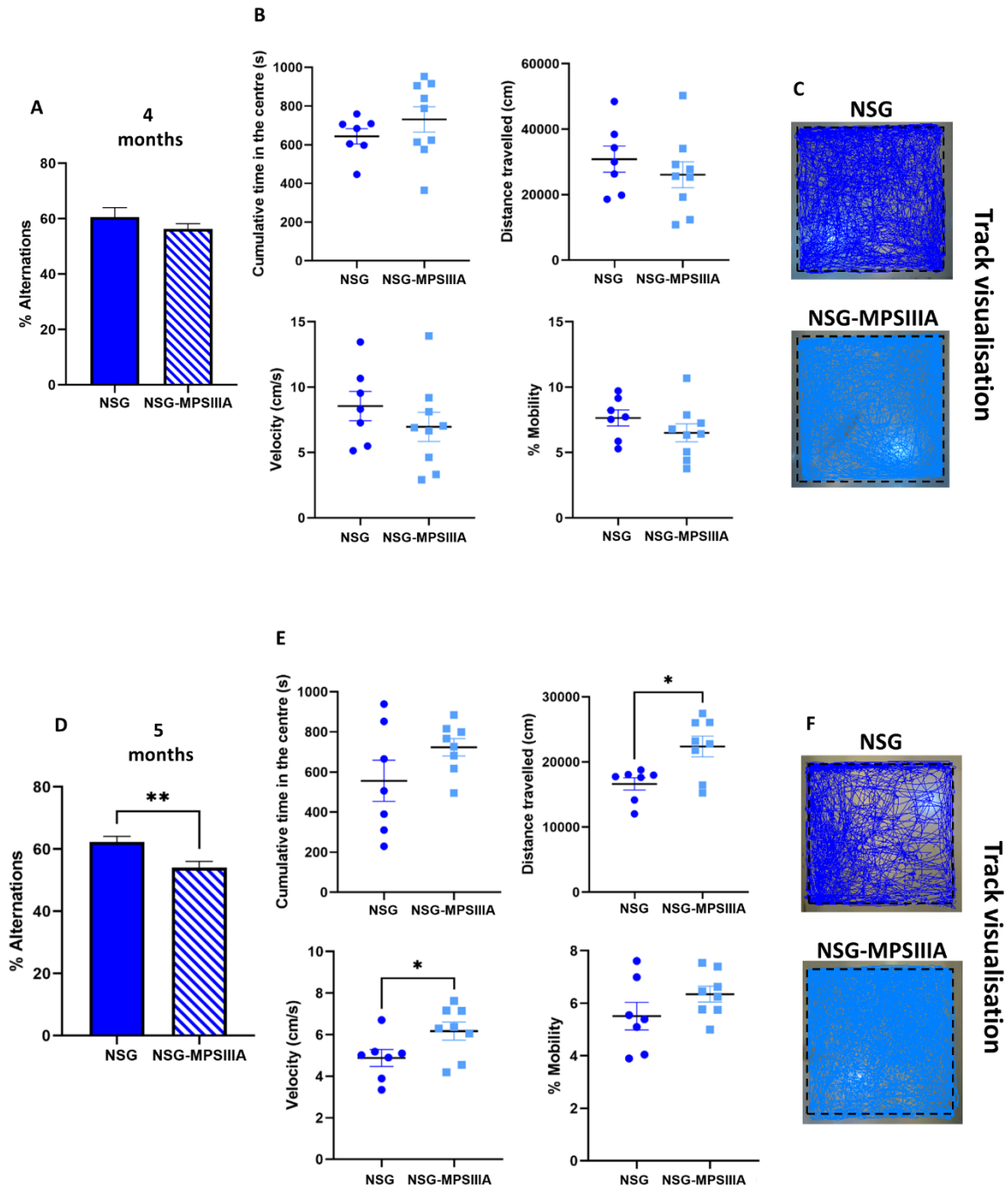
Figure 3: Female NSG-MPSIIIA mice exhibit impaired spatial working memory and hyperactivity Spontaneous alternation in the Y-maze was measured to assess working memory in NSG and NSG-MPSIIIA mice at 4 (**A**) and 5 (**D**) months of age. Mice were also placed in an open-field arena and the hyperactive behaviour was recorded for 60 minutes at 4 (**B**) and 5 (**E**) months of age using the following parameters: cumulative time in the centre, total distance travelled, velocity and % mobility. (**C, F**) Snapshots of representative open-field tracks are also displayed for each group. Error bars represent the standard error of the mean (SEM), n = 7-9. Significant differences are determined by unpaired t-test and are displayed above the line, *P < 0.05 and **P < 0.01.

NSG-MPSIIIA mice present reduced SGSH enzyme activity in the brain, enlarged lysosomal compartment and extensive astrogliosis

To investigate whether our NSG-MPSIIIA mouse model fully recapitulated the pathological features associated with the disease, we first measured the SGSH enzyme activity in the brain. In this respect, when compared to the WT littermates, our model displayed only 6% of WT SGSH enzyme activity (*Figure 4a*), which was comparable to B6-MPSIIIA mice. Since SGSH deficiency is known to lead to HS accumulation within the lysosome, we quantified the amount and composition of HS in the brain. In NSG mice, an average of 1.13 µg HS/mg protein was detected, increasing to 12.84-µg HS/mg protein in NSG-MPSIIIA animals, an increase by 11.4 fold (*Figure 4b*). A significant change in HS patterning was also observed with a 2.5-fold increase in the ΔHexA(2S)-GlcNS(6S) and a corresponding decrease in the non-sulphate disaccharide ΔHexA-GlcNAc (*Figure 4c*). To highlight lysosomal swelling as a consequence of storage of excess HS, coronal brain sections were stained for lysosomal associated membrane protein 2 (LAMP2), (*Figure 4d*). While in NSG brains, LAMP2 staining was punctate and surrounding the nuclei, NSG-MPSIIIA mice displayed significantly enlarged vesicular LAMP2+ lysosomes. Notably, the NSG-MPSIIIA mice presented a 2-fold increase in the % of LAMP2 stained area across several areas of the brain (cortex, striatum, hippocampus, amygdala), when compared to their WT littermates (*Figure 4e-h*). In addition, we also investigated whether this lysosomal impairment was accompanied by astrocytosis, as this has also been observed to be a marker of MPSIIIA disease (10). To do so, brain sections were also stained for the glial fibrillary acidic protein (GFAP), a marker of activated astrocytes. In NSGs, GFAP$^+$ cells were largely absent from the cortex and striatum, although staining was clearly visible in both hippocampus and amygdala *(Figure 4d).* Conversely, the NSG-MPSIIIA mice displayed a significant increase in astrocytic GFAP$^+$ cells in all the analysed brain areas, with fold increases varying from a minimum of 1.55 in the hippocampus and a maximum of 8 in the cortex (*Figure 4i-).*
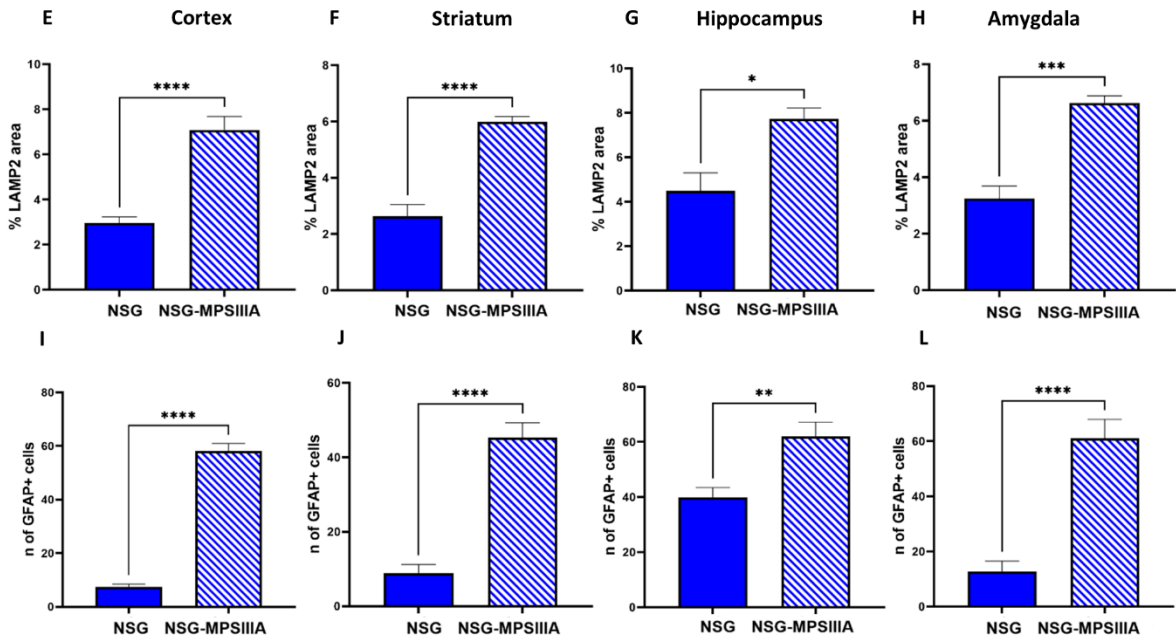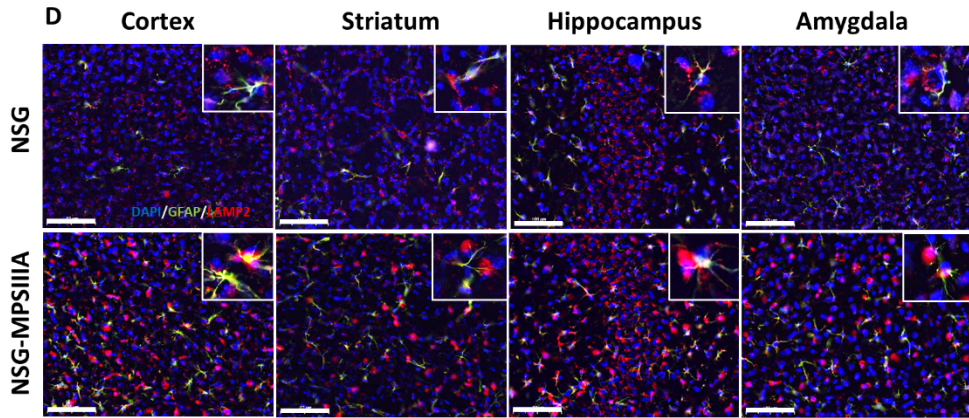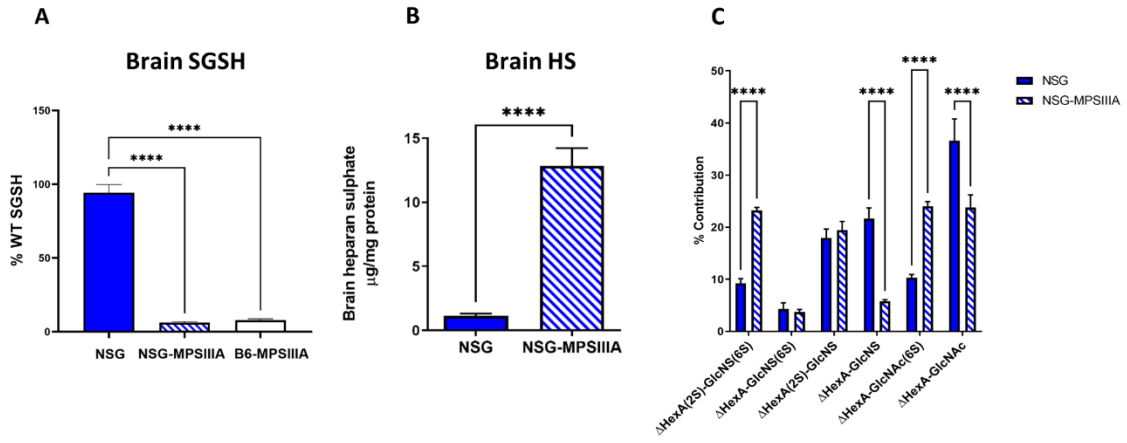
A Brain SGSH

B Brain HS

C

D

	Cortex	Striatum	Hippocampus	Amygdala
NSG				
NSG-MPSIIIA				

DAPI/GFAP/LAMP2

E Cortex

F Striatum

G Hippocampus

H Amygdala

I

J

K

L

Figure 4: NSG-MPSIIIA mice present reduced SGSH enzyme activity in the brain, enlarged lysosomal compartment and extensive astrogliosis.

(**A**) SGSH enzyme activity was measured in the brain of NSG,NSG-MPSIIIA and B6-MPSIIIA mice at 5 months of age. (B) HS quantification in the brain of NSG and NSG-MPSIIIA mice. (**C**) Disaccharide composition of HS in the brain of NSG and NSG-MPSIIIA mice. (**D**) Lysosomal enlargement and astrocytic activation were assessed at 5 months of age in both NSG and NSG-MPSIIIA mice via LAMP2-anf GFAP-labelling, respectively, in the cortex (covering layers IV/V/VI, from 0.02 to −2.70 relative to bregma), striatum (0.74 and 0.02 relative to bregma), hippocampus (−1.70 relative to bregma) and amygdala (−2.70 relative to bregma). Scale bar = 100 µm. Insets demonstrate representative astrocytes and lysosomal enlargement. % LAMP2 stained area was assessed by CellProfiler software in cortex (**E**), striatum (**F**), hippocampus (**G**) and amygdala (**H**). The number of GFAP+ cells was manually quantified in ImageJ in cortex (**I**), striatum (**J**), hippocampus (**K**) and amygdala (**L**). Error bars represent standard error of the mean (SEM), n = 6 in all groups. Significant differences were determined by by unpaired t-test, and are displayed above the line, $*P < 0.05$, $**P < 0.01$, $***P < 0.001$ and $****P < 0.0001$.

NSG-MPSIIIA mice display pronounced microglial activation

Extensive microgliosis is characteristic of MPSIIIA disease (10). In order to assess whether our mouse model was recapitulating this neuroinflammatory aspect, coronal brain sections were stained for isolectin B4 (ILB4), a marker of reactive microglia. In NSG mice, ILB4-positive cells were largely absent from the cortex, striatum and thalamic regions (*Figure 5a*). In contrast, NSG-MPSIIIA mice displayed between 80- and 107-fold increase in ILB4-positive microglia in several areas of the brain, including cortex, striatum, hippocampus and amygdala, indicative of extensive microgliosis (*Figure 5a-e).*
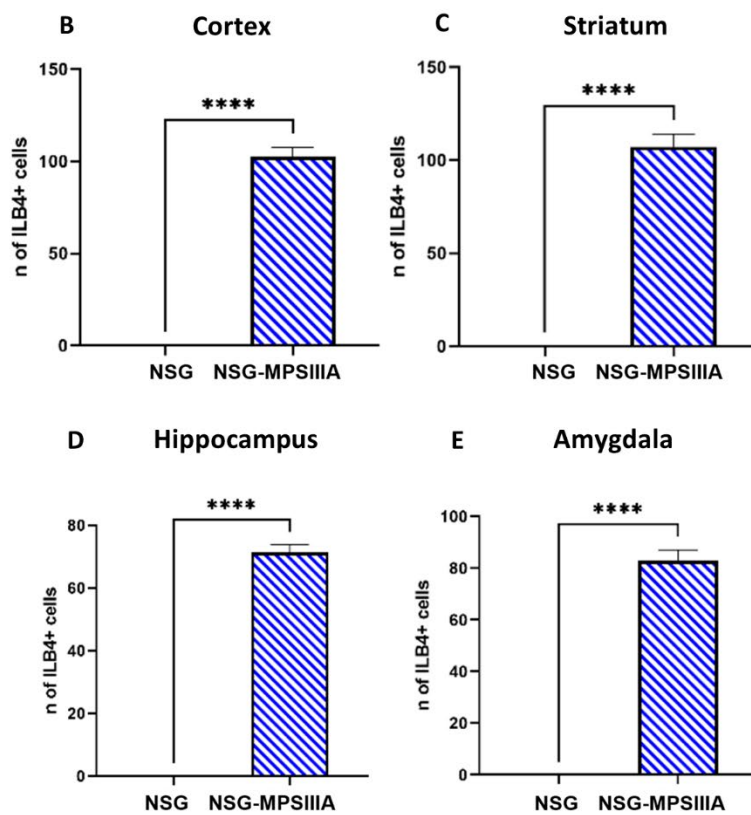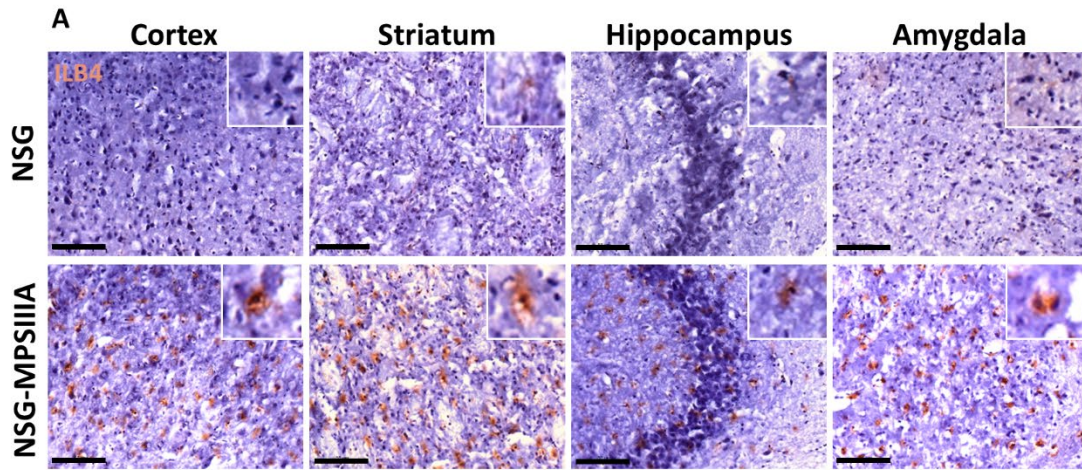
Figure 5: MPS IIIA/NSG mice display pronounced microglia activation

(**A**) Microglial activation was assessed at 5 months of age in both NSG and NSG-MPSIIIA mice via isolectin-B4 labelling in the cortex (covering layers IV/V/VI, from 0.02 to −2.70 relative to bregma), striatum (0.74 and 0.02 relative to bregma), hippocampus (−1.70 relative to bregma) and amygdala (−2.70 relative to bregma). Scale bar = 100 μm. Insets demonstrate representative microglia. The number of ILB4+ cells was manually quantified in ImageJ in cortex (**B**), striatum (**C**), hippocampus (**D**) and amygdala (**E**). Error bars represent standard error of the mean (SEM), n = 6 in all groups. Significant differences were determined by by unpaired t-test, and are displayed above the line, *P < 0.05, **P < 0.01, ***P < 0.001 and ****P < 0.0001.

NSG-MPSIIIA mice show evidence of human neural progenitor engraftment

To assess the potential of human stem cell-based products to engraft, survive and migrate in the CNS of NSG-MPSIIIA mice, we transplanted unaffected iPSC-derived NPCs into the striatum of 2-month-old NSG-MPSIIIA mice (2×10^5 cells per animal; one injection per hemisphere) (*Figure 6a*). Engrafted human cells were detected by an antibody that specifically recognises human nuclear proteins (H-NUCLEI). Analysis performed at 3 months post-injection revealed the unaffected NPCs were more commonly found in the brain sections close to the injection site and were found in proximity of the external capsule (*Figure 6a,b*). Notably, positive staining was not only found in the striatum, but also in several other areas of the brain, such as the lateral ventricle, ventral pallidum, striata terminalis and alveus (*Figure 6c*).
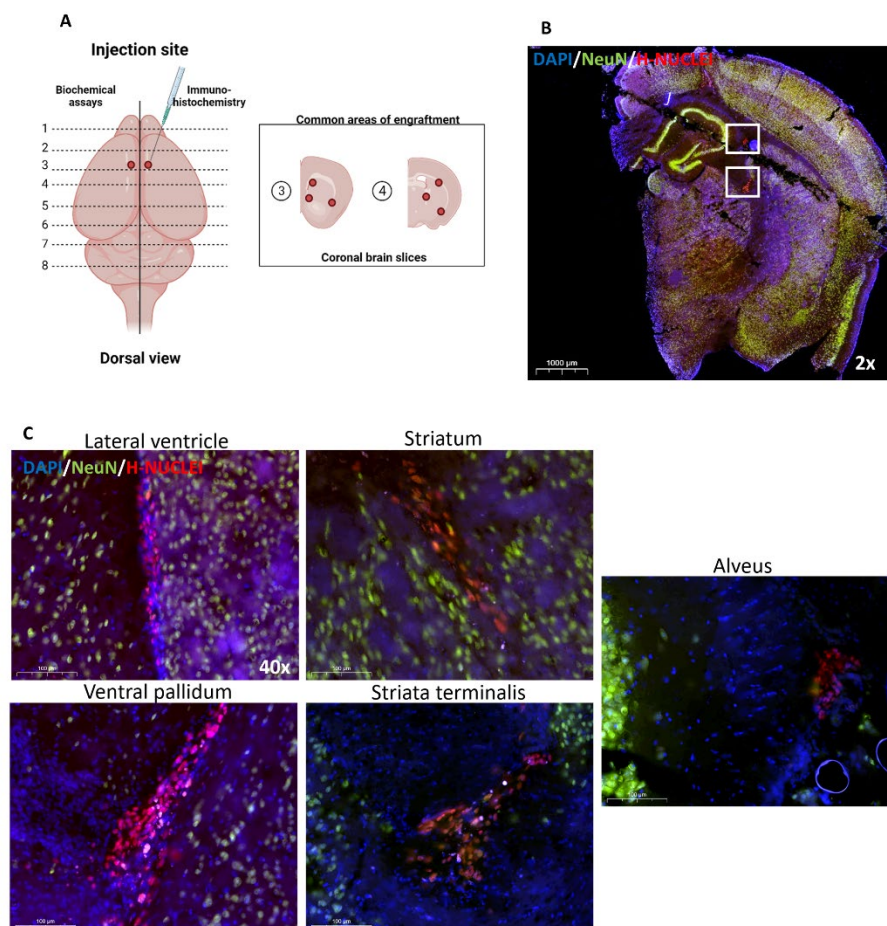
Figure 6: NSG-MPSIIIA mice show evidence of human neural progenitor engraftment
(**A**) Schematic representing the injection site (2 mm lateral to bregma; 3 mm depth from the cerebral surface) and the preferred area of cell engraftment (+0.74 mm and +0.02 mm relative to bregma). At harvest, one bran hemisphere was snap-frozen for biochemical assays, while the other was fixed for immunohistochemistry. (**B,C**) H-NUCLEI positive iPSC-derived NPCs (red), nuclei (DAPI) and NeuN positive mouse neurons (green) in several regions of the NSG-MPSIIIA mice brain (0.74 to -2.70 relative to bregma). Representative images are shown following staining. Scale bars = 1000 – 100 μm**.**

Discussion

The aim of this study was to generate and characterise a highly immunodeficient mouse model of disease that could serve as a future platform to test human stem-cell based products. To achieve this, we crossed MPSIIIA (B6.Cg-*Sgsh*^mps3a/6J) mutant males with NOD.Cg-*Prkdc*^Scid *Il2rg*^tm1Wjl/SzJ (NSG) females and the obtained heterozygous offspring were backcrossed to NSG mice for five generations. Notably, in the sixth generation, backcrossing onto NSG was not fully complete (~95.31%), leading to potential heterogeneity in the offspring with respect to the NOD genotype. To reduce this residual genotype in future studies, mice will be further backcrossed.

Our findings show that our NSG-MPSIIIA mouse model inherited the distinctive immunodeficient profile of NSG mice (16), marked by compromised adaptive immunity. This characteristic ultimately facilitated the successful engraftment of human iPSC-derived NPCs in the brain, leading to survival for up to three months post-delivery. Furthermore, female NSG-MPSIIIA mice also exhibited impaired spatial working memory, reduced thigmotaxis and hyperactive behaviour at 5 months of age – traits consistent with the behavioural phenotype observed in MPSIIIA patients and MPSIIIA mice (4). Lastly, NSG-MPSIIIA mice also displayed pronounced neuropathology, including GAG accumulation and altered sulphation patterning in the brain, lysosomal enlargement and gliosis, aligning with observations in several other MPS mouse models (10).

We initially characterised the immune system profile of our newly generated NSG-MPSIIIA mice, in order to confirm their suitability for xenotransplantation. When compared to WTs, NSG-MPSIIIA mice exhibited lack of functional B cells, T cells and NK cells across blood, spleen and thymus, mirroring the observations in the parental NSG (16). Notably, lack of NK cells represent a crucial advantage when compared to other immunodeficient MPS mice, such as the NOD/SCID MPSVII (22) and NOD/SCID MPSI (15) mouse models, as NK cells are known to contribute to both acute and chronic graft rejection (23). This deficiency was also achieved in a recently generated MPSIIIA Triple knockout (B6.129S-*Rag2*^tm1Fwa *Cd47*^tm1Fpl *Il2rg*^tm1Wjl/J; MPSIIIA-TKO) mouse model (24). While exhibiting tolerance to xenotransplantation, this model displays a less profound immunodeficiency when compared to NSGs, which remain the preferred choice for xenotransplantation studies. In fact, NSGs are also marked by the absence of lymphoid cells and splenic follicles, reduced lymph nodes cellularity and lack of serum Ig (25, 26).

Additionally, we also sought to gain an insight into the role of the immune system in disease pathology and behaviour. NSG-MPSIIIA splenocytes, thymus and white blood cell populations

did not display any significant differences when compared to NSGs, with low or absent B, T and NK cells as expected, except that circulating monocytes dropped in NSG-MPSIIIAs against NSGs. The CCL5 (RANTES) chemokine is recognised as a key driver of monocyte trafficking and recruitment (27). Importantly, previous studies indicated that soluble HS inhibits the binding of RANTES to its cognate receptor CCR5 (28). Consequently, the elevated levels of soluble HS in MPS IIIA disease could potentially impede the CCL5-CCR5 axis, thereby resulting in a diminished trafficking of monocytes from the bone marrow. There is existing evidence suggesting a key role for innate immune activation in the brain, particularly microglia, in MPSIIIA neuropathology progression, and this has been extensively reviewed (11, 29). In this regard, widespread microgliosis and astrogliosis were detected in several brain areas of 5-month old NSG-MPSIIIA mice when compared to their NSG littermates; this is in line with ourselves and other groups reporting considerable gliosis in both neuronopathic MPS patients and mouse models (10, 30-32). The neuroinflammatory phenotype in MPSIIIA-TKO mice was not described, ultimately hampering the possibility of making further comparisons. However, there was a documented presence of cytoplasmic microvesiculation affecting epithelia, macrophages and neurons, along with evidence of undetectable SGSH activity in the brain (24). This observation aligns with the characteristics of lysosomal storage disorders and is congruent with our findings, where mice displayed an enlarged lysosomal compartment, presumably due to GAG accumulation in the brain.

Although there is limited published data regarding the role of adaptive immunity in MPS diseases, studies on MPSIIIB mice provide evidence of an adaptive immune contribution to disease pathogenesis (33, 34). In particular, MPSIIIB lymphocytes proved to trigger neuroinflammation following implantation into naïve WT mice (34), although further elucidation on the role of T cells is required. Conversely, MPSI mice displayed adaptive immune dysfunction when compared to WT controls (35), suggesting specific immunological features associated with each MPS type. In the case of our MPSIIIA/NSG model the lack of adaptive immune responses (abrogated by the NSG phenotype), did not seem to have an implication on MPSIIIA disease progression, as by 5 months of age NSG-MPSIIIA mice still displayed extensive brain inflammation, ultimately supporting our previous hypothesis that neuropathology in this model is primarily innate immunity-driven (29, 36).

Having full abrogation of the adaptive immune response in NSG-MPSIIIA mice allowed efficient intracranial delivery of human iPSC-derived NPCs and engraftment for up to three months post-injection, with no tumour onset. In this respect, recently generated NSG-MPSI mouse models also allowed long-term engraftment of human neural stem cells in the brain (20, 37). The yield of NPC engraftment in the CNS of NSG-MPSIIIA mice was highly variable,

with higher % of engraftment close to the injection site. The cells also exhibited a distinct preference for migration through white matter tracts and the ventricular system, similarly to what has been reported by other groups (24, 38).

Only female mice were used in our behavioural analysis, due to the fact that only MPSIIIA female mice had been reported to recapitulate the behavioural abnormalities observed in patients, including cognitive decline (11) and hyperactivity (9). With regards to cognitive function, NSG-MPSIIIA mice displayed significant spatial working memory deficits at 5 months of age when compared to their NSG littermates. In this respect, similar levels of memory impairment were also reported in MPSIIIA mice at 6 months of age (11). NSG-MPSIIIA mice also displayed significant hyperactivity at 5 months of age, although this significance seemed to be due to NSG mice experiencing decreased locomotor activity with aging, as opposed to NSG-MPSIIIA, which retained the same activity levels. In this regard, aging in mice is known to lead to progressive changes in cognition and was proved to be associated with reduced motor function in WT mice (39). Although hyperactivity levels were similar to the ones observed in the MPSIIIA model, the latter showed a significant phenotype as early as 4 months of age (9). This is in contrast to a study conducted by *Crawley et al*, reporting no difference in hyperactivity between WT and MPSIIIA mice prior to 18 weeks of age (40), which is in line with our findings. In addition, both mouse models shared a potential reduced sense of danger, observed by increased time spent in the centre of the open-field arena (9), which is also often a characteristic of MPSIIIA patients (4). This differs with what was reported in an Alzheimer's disease (AD) study, in which female AD mice spent less time in the centre of the open-field, ultimately indicating increased anxiety-like behaviour (41).

In conclusion, NSG-MPSIIIA mice emerged as a potent platform for evaluating the efficacy of human stem cell-based therapies in treating MPSIIIA, paving the way for future research in this area.

Materials and Methods

Maintenance of mouse colonies

All animal work was performed with local ethical approval and in accordance with Home Office regulations. All Schedule 1 procedures were performed in accordance with the Animals (Scientific Procedures) Act, 1986 (UK), under project licence PPL P0C3AEEB0 and approved by the University of Manchester Ethical Review Process Committee. Mice were housed in groups of 2-5 under specific-pathogen-free (SPF) conditions, with a regular 12/12-hour light/dark cycle, under controlled temperature and light. They were provided with irradiated food and sterile deionized water ad libitum. NOD.Cg-$Prkdc^{scid}$ $Il2rg^{tm1Wjl}$/Sgsh^{mps3a}/6J (NSG-MPSIIIA) mice were generated by crossing MPSIIIA (B6.Cg-Sgsh^{mps3a}/6J) mutant males with NOD.Cg-$Prkdc^{scid}$ $Il2rg^{tm1Wjl}$/SzJ (NSG) females for five generations. MPSIIIA mice mutant for *PRKDC* and *IL2RG* were maintained by heterozygote breeding, generating WT and MPSIIIA littermates, genotyping as previously described (12, 42).

Experimental Analysis

NSG and NSG-MPSIIIA female mice were compared against each other for both behavioural and histochemical analyses. Histology, biochemistry and behavioural analyses were carried out on n = 3–9. N numbers were based on previous power calculations (12, 32, 42). Behavioural tests were recorded and analysed at a later time-point from video in a blinded fashion once all tests had been performed. Data analysis was carried out in a blinded fashion.

Y-maze spontaneous alternations

Spontaneous alternation was assessed during one continuous 10 min session in a Y-maze consisting of three identical arms as previously described (42). The behaviour was recorded for 10 minutes using a digital camcorder (Sony) and analysed manually.

Open-field test

Female mice were analysed using the open-field test, as previously described (9). All open-field tests were performed 1.5 hours into the 12-hour light cycle. Mice were placed in the centre of a matt white acrylic open-field arena (Width: 450 mm, depth: 450 mm, height: 500 mm, 127 lux), recorded for 60 minutes. Cumulative time in the centre, distance travelled, velocity and mobility were analysed using Ethovision XT11.5 software (Noldus, Wageningen, the Netherlands).

iPSCs generation and differentiation into NPCs

Normal human dermal fibroblasts (C0045C, ThermoFisher Scientific, Altrincham, UK) were reprogrammed into iPSCs by a single transfection with oriP/EBNA-based episomal vectors using the human dermal fibroblast nucleofector™ Kit (VPD-1001, Lonza, Basel, Switzerland), according to the manufacturer's instructions. iPSCs were then differentiated to NPCs in 7 days, by culture in complete PSC neural induction medium (A1647801, ThermoFisher Scientific), according to the manufacturer's instructions. Successful differentiation into NPCs was assessed via immunofluorescent staining and qPCR analysis for the expression of NPC markers, including *PAX6, SOX2 and NESTIN*.

Stereotactic injection of NPCs

Before surgery, buprenorphine was diluted 1:10 with saline on the day of use. The mouse's weight was recorded prior to the procedure, which was conducted aseptically. NSG mice were anesthetized with isoflurane (4% induction in 4L/min O2, then 2% maintenance in 2L/min), then moved to the surgical area and placed on a heated pad in a stereotactic apparatus. Anesthesia was confirmed with a toe pinch reflex, and physiological parameters were monitored. The mice's heads were cleaned with Videne and ethanol, a midline incision was made, and the dura mater removed. Bregma was identified, marked, and measured with a Vernier scale. A hole was drilled 2 mm lateral to bregma over the right striatum. Using a sterile Hamilton syringe with a 26G needle, 7 μl of cell suspension (2×10^5 unaffected NPC per mouse; one injection per hemisphere; 3 mm depth from the cerebral surface) or saline was injected. The injection was done over 5 minutes, and PBS (100 μl) and 0.1 mg/kg buprenorphine (100 μl) were administered subcutaneously. The needle was retracted, another hole drilled in the opposite hemisphere, and the procedure repeated. The skin was closed with absorbable sutures. Post-surgery, the mice were placed in a recovery cage with food and water, monitored until fully awake, and observed daily. At 3 months after injection, animals were culled and brains harvested for histological analysis.

Tissue harvesting and cell isolation

Anesthetised animals received an intra-cardiac perfusion of PBS, tissues were harvested and brains processed as previously described (12). Spleens were finely chopped and digested for 30 minutes at 37°C with gentle shaking at 150 rpm in an enzyme cocktail (HANKs (Sigma, H9269) containing 0.5% penicillin/streptomycin solution, 0.4 U/ml liberase TL (Sigma) + 80 U/ml DNase (Sigma)). EDTA (Sigma) was added to a final concentration of 10 mM and samples diluted with flow buffer (PBS + 1% FBS). Digested spleens were passed through a

70 μm pore cell strainer. Splenocytes were treated with RBC lysis buffer (Sigma) for 3 minutes at room temperature, washed with flow buffer, after which cells were ready for staining. The thymus was passed through a 100 μm pore strainer and the sample washed through the strainer with flow buffer. Following a 10-minute incubation with RBC lysis buffer on ice, samples centrifugation at 230 g for 10 minutes at 4°C, before resuspension in flow buffer. The blood was centrifuged at 200 g for 10 minutes at 4°C and the supernatant (plasma) stored at – 80°C. White blood cells (WBCs) were re-suspended in 1 ml RBC lysis buffer, incubated on ice for 10 minutes and centrifuged at 200 x g, 4°C for 10 minutes. Following repetition of the RBC lysis step, the WBCs were washed with 500 μl 1xPBS/2% FBS and centrifuged at 200 x g, 4°C for 10 minutes. The supernatant was removed and the pellet resuspended in flow buffer.

Flow cytometry analysis

Samples were washed with PBS and stained for viability with ZombieUV (1:2,000; Biolegend). Samples were then blocked with 5 μg/ml αCD16/CD32 (2.4G2; BioLegend) in FACS buffer (PBS containing 2% FBS and 2 mM EDTA) before staining for surface markers at 4°C (BioLegend) for 30 minutes (*Table 1*). After staining, cells were washed twice in FACS buffer and then fixed in 1% paraformaldehyde in PBS for 10 min at room temperature. Samples were acquired on BD Fortessa or LSRII flow cytometers with FACSDiva™ (BD Biosciences) software. Effective compensation was achieved, standardised PMT voltages based on CST were applied prior to acquisition. Data was analysed with FlowJo v10 (Tree Star). A gating schemes of murine immune cell populations is provided (*Supplementary Figure 1*).

Table 1: Information regarding the antibodies used for flow cytometry analysis

Antigen	Conjugate	Dilution	Clone
CD209b	FITC	1:100	22D1
Tim4	PerCP/eF710	1:100	RMT4-54
CD169	APC	1:100	3D6-112
Ly6C	AF700	1:200	HK1.4
Lineage*	APC/eFluor780	1:200	
CD64	BV421	1:200	X54-5/7.1
XCR1	BV510	1:400	ZET
CD11c	BV605	1:600	N418
CD86	BV650	1:200	GL-1
CD11b	BV711	1:1000	M1/70
CD45	BV785	1:200	A20
F4/80	PE	1:100	BM8
MHCII	PE/Cy5	1:200	M5/114.15.2
CD68	PE/Cy7	1:100	FA-11
NK1.1	APC/eFluor780	1:200	PK136
CD4	BV421	1:200	RM4-5
CD8	BV785	1:200	53-6.7

* Lineage: [Ly6g (clone IA8), CD3 (clone I7A2), TCRβ (clone H57-597), CD19 (clone (1D3) 605)]

SGSH enzyme activity

SGSH enzyme activity was measured in a two-step protocol using a fluorescent substrate MU-αGlcNS (Moscerdam, Oegstgeest, the Netherlands) as per manufacturer's instructions (43).

Heparan sulphate quantification

HS amounts and patterning was measured as described previously in (44) using reverse phase-HPLC following 2-aminoacridone labelling of heparinase-digested HS chains.

IHC analysis of mouse brain

Cutting brain Sections on Microtome

Mouse brains following perfusion were fixed for 24 hours in 4 % PFA, then transferred to 30% sucrose/-2 mM MgCl2 for 24 hours. The brains were then stored in aluminium pouches at - 80 °C. Brain tissue sections (30 µm) were cut on a freezing microtome in optimal cutting temperature compound (KP-CryoCompound, 1620C, Klinipath, Duiven, Netherlands), after removing cerebellum and olfactory bulb, and stored at 4 °C in anti-freeze TRIS buffered saline (TBS-AF) (TBS-A: TBS + 0.05% NaN_3; TBS-AF: 350 mL TBS-A, 75 g sucrose, 150 mL ethylene glycol) in round-bottomed 96 well plates.

Free-floating IHC

Free-floating IHC was performed on 30 µm PFA-fixed coronal brain sections using rabbit anti-GFAP (1:1500, Z0334, Dako, Stockport, UK), rat anti-LAMP2 (1:500, ab13524, Abcam), mouse anti-NeuN (1:1000, ab104224, Abcam) and mouse anti-Nuclei clone 235-1 (1:100, MAB1281, Sigma-Aldrich) primary antibodies using standard protocols (45). ILB4 (5µg/ml, L5391, Sigma-Aldrich) was visualized on 30 µm coronal brain sections using DAB substrate for 40 seconds (Vector, Peterborough, UK), as previously described (10). Images were acquired on a 3D-Histech Pannoramic-250 microscope slide-scanner using a 40x/0.30 Plan Achromat objective (Zeiss) with extended focus and the DAPI, FITC and TRITC filter sets. Snapshots of the slide-scans were taken using Slide Viewer software (3D-Histech). Nonlinear adjustments were made to all immunofluorescence images equally to eliminate background. GFAP+ and ILB4+ cells were quantified in cortex, striatum, amygdala and hippocampus at 40x magnification (n=6/group) by ImageJ software. Fluorescent quantification of LAMP2 (in cortex, striatum, amygdala and hippocampus – 40x magnification) positive staining (% stained area) was performed using CellProfiler software (n=6/group).

*Statistical Analysis*

Statistical analysis was performed using GraphPad Prism 9 software (La Jolla, CA, USA). Comparisons between two groups were performed by two-tailed unpaired t-test. One-way analysis of variance (ANOVAs) were applied for multi-group analysis, followed by Tukey's multiple comparison test. Significance was set at $P < 0.05$ %. Data are presented as standard error of the mean (SEM).

References

1.   Valstar MJ, Ruijter GJG, Van Diggelen OP, Poorthuis BJ, Wijburg FA. Sanfilippo syndrome: A mini-review. Journal of Inherited Metabolic Disease. 2008;31(2):240-52.
2.   Disorders NOfR. Mucopolysaccharidosis Type III   [Available from: https://rarediseases.org/rare-diseases/mucopolysaccharidosis-type-iii/.
3.   Valstar MJ, Neijs S, Bruggenwirth HT, Olmer R, Ruijter GJG, Wevers RA, et al. Mucopolysaccharidosis type IIIA: Clinical spectrum and genotype-phenotype correlations. Annals of Neurology. 2010;68(6):876-87.
4.   Muenzer J. Overview of the mucopolysaccharidoses. Rheumatology (Oxford). 2011;50 Suppl 5:v4-12.
5.   Sivakumur P, Wraith JE. Bone marrow transplantation in mucopolysaccharidosis type IIIA: A comparison of an early treated patient with his untreated sibling. Journal of Inherited Metabolic Disease. 1999;22(7):849-50.
6.   Shapiro EG, Jones SA, Escolar ML. Developmental and behavioral aspects of mucopolysaccharidoses with brain manifestations - Neurological signs and symptoms. Mol Genet Metab. 2017;122S:1-7.
7.   Mandolfo O, Bigger BW. Gene-modified neural progenitor cells for the treatment of neuropathic lysosomal storage diseases. Neural Regen Res. 2023;18(9):1954-5.
8.   Bhaumik M, Muller VJ, Rozaklis T, Linda J, Dobrenis K, Bhattacharyya R, et al. A mouse model for mucopolysaccharidosis type III A (Sanfilippo syndrome). Glycobiology. 1999;9(12):1389-96.
9.   Langford-Smith A, Langford-Smith KJ, Jones SA, Wynn RF, Wraith JE, Wilkinson FL, et al. Female mucopolysaccharidosis IIIA mice exhibit hyperactivity and a reduced sense of danger in the open field test. PLoS One. 2011;6(10):e25717.
10.   Wilkinson FL, Holley RJ, Langford-Smith KJ, Badrinath S, Liao A, Langford-Smith A, et al. Neuropathology in Mouse Models of Mucopolysaccharidosis Type I, IIIA and IIIB. PLoS ONE. 2012;7(4):e35787.
11.   Parker H, Ellison SM, Holley RJ, O'Leary C, Liao A, Asadi J, et al. Haematopoietic stem cell gene therapy with IL1Ra rescues cognitive loss in mucopolysaccharidosis IIIA. EMBO Molecular Medicine. 2020;12(3).
12.   Sergijenko A, Langford-Smith A, Liao AY, Pickford CE, Mcdermott J, Nowinski G, et al. Myeloid/Microglial Driven Autologous Hematopoietic Stem Cell Gene Therapy Corrects a Neuronopathic Lysosomal Disease. Molecular Therapy. 2013;21(10):1938-49.
13.   Ellison SM, Liao A, Wood S, Taylor J, Youshani AS, Rowlston S, et al. Pre-clinical Safety and Efficacy of Lentiviral Vector-Mediated Ex Vivo Stem Cell Gene Therapy for the Treatment of Mucopolysaccharidosis IIIA. Molecular Therapy - Methods & Clinical Development. 2019;13:399-413.
14.   ISSCR Guidelines   [Available from: https://www.isscr.org/guidelines/blog-post-title-one-ed2td-6fcdk-5zr5l.
15.   Garcia-Rivera MF, Colvin-Wanshura LE, Nelson MS, Nan Z, Khan SA, Rogers TB, et al. Characterization of an immunodeficient mouse model of mucopolysaccharidosis type I suitable for preclinical testing of human stem cell and gene therapy. Brain Research Bulletin. 2007;74(6):429-38.
16.   Ito M, Hiramatsu H, Kobayashi K, Suzue K, Kawahata M, Hioki K, et al. NOD/SCID/gamma(c)(null) mouse: an excellent recipient mouse model for engraftment of human cells. Blood. 2002;100(9):3175-82.
17.   Tian X, Woll PS, Morris JK, Linehan JL, Kaufman DS. Hematopoietic Engraftment of Human Embryonic Stem Cell-Derived Cells Is Regulated by Recipient Innate Immunity. STEM CELLS. 2006;24(5):1370-80.
18.   Lobo De Figueiredo-Pontes L, Adamcova MK, Grusanovic S, Kuzmina M, Aparecida Lopes I, Fernandes De Oliveira Costa A, et al. Improved hematopoietic stem cell transplantation upon inhibition of natural killer cell-derived interferon-gamma. Stem Cell Reports. 2021;16(8):1999-2013.
19.   Xia X, Li H, Satheesan S, Zhou J, Rossi JJ. Humanized NOD/SCID/IL2rγnull (hu-NSG) Mouse Model for HIV Replication and Latency Studies. Journal of Visualized Experiments. 2019(143).
20.   Mendez DC, Stover AE, Rangel AD, Brick DJ, Nethercott HE, Torres MA, et al. A novel, long-lived, and highly engraftable immunodeficient mouse model of mucopolysaccharidosis type I. Molecular Therapy - Methods & Clinical Development. 2015;2:14068.
21.   Di Santo JP, Vosshenrich CAJ. Bone marrow versus thymic pathways of natural killer cell development. Immunological Reviews. 2006;214(1):35-46.
22.   Griffin A, Tagan, Anderson C, Hayley, Wolfe H, John. Ex Vivo Gene Therapy Using Patient iPSC-Derived NSCs Reverses Pathology in the Brain of a Homologous Mouse Model. Stem Cell Reports. 2015;4(5):835-46.
23.   Benichou G, Yamada Y, Aoyama A, Madsen JC. Natural killer cells in rejection and tolerance of solid organ allografts. Current Opinion in Organ Transplantation. 2011;16(1):47-53.
24.   Pollock K, Noritake S, Imai DM, Pastenkos G, Olson M, Cary W, et al. An immune deficient mouse model for mucopolysaccharidosis IIIA (Sanfilippo syndrome). Scientific Reports. 2023;13(1).

25.   Shultz LD, Lyons BL, Burzenski LM, Gott B, Chen X, Chaleff S, et al. Human Lymphoid and Myeloid Cell Development in NOD/LtSz-*scid IL2R*γ*null* Mice Engrafted with Mobilized Human Hemopoietic Stem Cells. The Journal of Immunology. 2005;174(10):6477-89.

26.   Shultz LD, Brehm MA, Garcia-Martinez JV, Greiner DL. Humanized mice for immune system investigation: progress, promise and challenges. Nature Reviews Immunology. 2012;12(11):786-98.

27.   Gerhardt T, Ley K. Monocyte trafficking across the vessel wall. Cardiovascular research. 2015;107(3):321-30.

28.   Loıc Martin CB, Pascale Garnier, Valerie Wittamer, Marc Parmentier, and Claudio Vita. Structural and Functional Analysis of the RANTES-GlycosaminoglycansInteractions. Biochemistry. 2001;40:6303-631810.1021/bi002670n CCC: $20.00© 2001 American Chemical SocietyPublished on Web 05/04/2001.

29.   Mandolfo O, Parker H, Bigger B. Innate Immunity in Mucopolysaccharide Diseases. International Journal of Molecular Sciences. 2022;23(4):1999.

30.   Viana GM, Priestman DA, Platt FM, Khan S, Tomatsu S, Pshezhetsky AV. Brain Pathology in Mucopolysaccharidoses (MPS) Patients with Neurological Forms. Journal of Clinical Medicine. 2020;9(2):396.

31.   Ohmi K, Greenberg DS, Rajavel KS, Ryazantsev S, Li HH, Neufeld EF. Activated microglia in cortex of mouse models of mucopolysaccharidoses I and IIIB. Proceedings of the National Academy of Sciences. 2003;100(4):1902-7.

32.   Gleitz HF, Liao AY, Cook JR, Rowlston SF, Forte GM, D'Souza Z, et al. Brain-targeted stem cell gene therapy corrects mucopolysaccharidosis type II via multiple mechanisms. EMBO Molecular Medicine. 2018;10(7):e8730.

33.   Dirosario J, Divers E, Wang C, Etter J, Charrier A, Jukkola P, et al. Innate and adaptive immune activation in the brain of MPS IIIB mouse model. Journal of Neuroscience Research. 2009;87(4):978-90.

34.   Killedar S, Dirosario J, Divers E, Popovich PG, Mccarty DM, Fu H. Mucopolysaccharidosis IIIB, a lysosomal storage disease, triggers a pathogenic CNS autoimmune response. Journal of Neuroinflammation. 2010;7(1):39.

35.   Archer LD, Langford-Smith KJ, Bigger BW, Fildes JE. Mucopolysaccharide diseases: A complex interplay between neuroinflammation, microglial activation and adaptive immunity. Journal of Inherited Metabolic Disease. 2014;37(1):1-12.

36.   Parker H, Bigger BW. The role of innate immunity in mucopolysaccharide diseases. Journal of Neurochemistry. 2019;148(5):639-51.

37.   Gomez-Ospina N, Scharenberg SG, Mostrel N, Bak RO, Mantri S, Quadros RM, et al. Human genome-edited hematopoietic stem cells phenotypically correct Mucopolysaccharidosis type I. Nature Communications. 2019;10(1).

38.   Meneghini V, Frati G, Sala D, De Cicco S, Luciani M, Cavazzin C, et al. Generation of Human Induced Pluripotent Stem Cell-Derived Bona Fide Neural Stem Cells for Ex Vivo Gene Therapy of Metachromatic Leukodystrophy. Stem Cells Translational Medicine. 2017;6(2):352-68.

39.   Shoji H, Takao K, Hattori S, Miyakawa T. Age-related changes in behavior in C57BL/6J mice from young adulthood to middle age. Molecular Brain. 2016;9(1).

40.   Crawley AC, Gliddon BL, Auclair D, Brodie SL, Hirte C, King BM, et al. Characterization of a C57BL/6 congenic mouse strain of mucopolysaccharidosis type IIIA. Brain Res. 2006;1104(1):1-17.

41.   Szabó A, Farkas S, Fazekas C, Correia P, Chaves T, Sipos E, et al. Temporal Appearance of Enhanced Innate Anxiety in Alzheimer Model Mice. Biomedicines. 2023;11(2):262.

42.   Langford-Smith A, Wilkinson FL, Langford-Smith KJ, Holley RJ, Sergijenko A, Howe SJ, et al. Hematopoietic Stem Cell and Gene Therapy Corrects Primary Neuropathology and Behavior in Mucopolysaccharidosis IIIA Mice. Molecular Therapy. 2012;20(8):1610-21.

43.   Karpova EA, Voznyi YV, Keulemans JLM, Hoogeveen AT, Winchester B, Tsvetkova IV, et al. A fluorimetric enzyme assay for the diagnosis of sanfilippo disease type A (MPS IIIA). Journal of Inherited Metabolic Disease. 1996;19(3):278-85.

44.   Holley RJ, Ellison SM, Fil D, O'Leary C, McDermott J, Senthivel N, et al. Macrophage enzyme and reduced inflammation drive brain correction of mucopolysaccharidosis IIIB by stem cell gene therapy. Brain. 2018;141(1):99-116.

45.   Malinowska M, Wilkinson FL, Langford-Smith KJ, Langford-Smith A, Brown JR, Crawford BE, et al. Genistein Improves Neuropathology and Corrects Behaviour in a Mouse Model of Neurodegenerative Metabolic Disease. PLoS ONE. 2010;5(12):e14192.

Supplementary Material
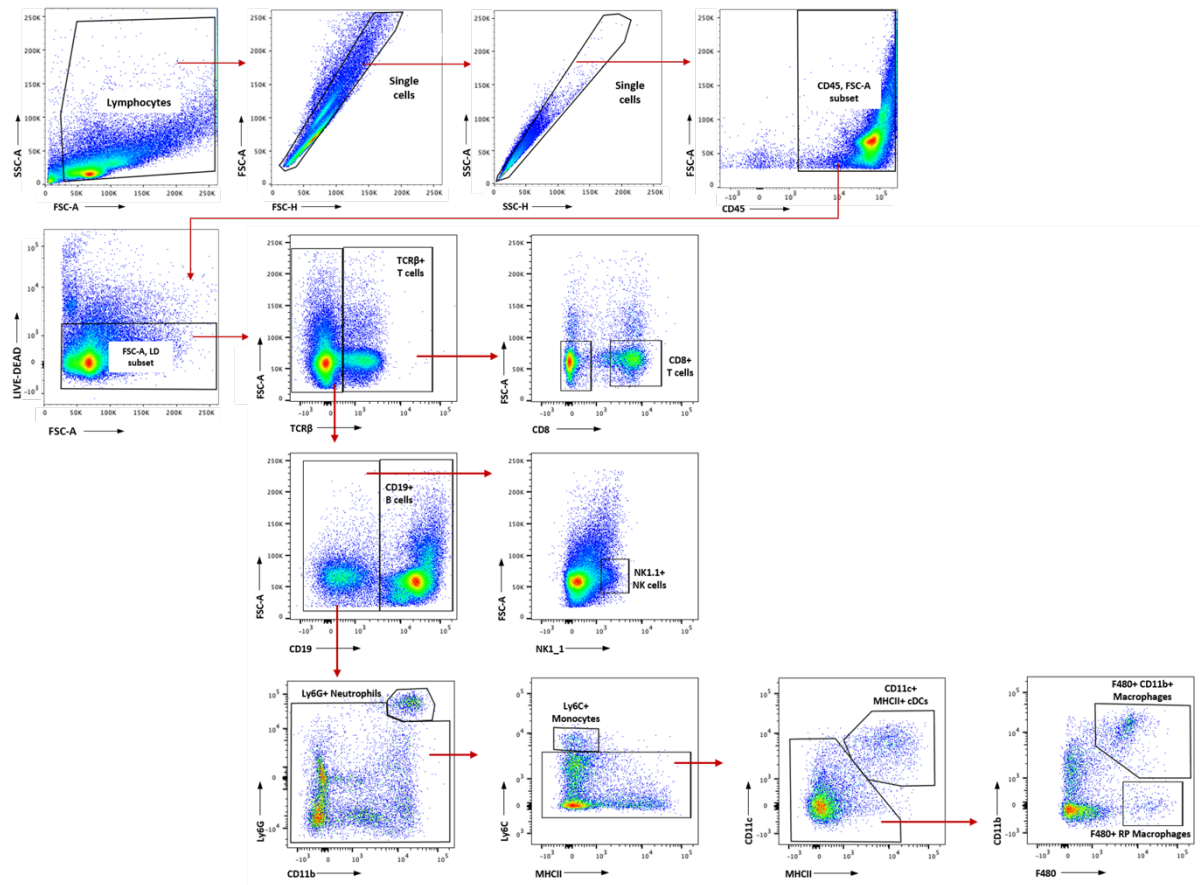
Supplementary figure 1: Gating strategy for adaptive and innate immune cells

Whole tissue digests were prepared following tissue harvest. Cells were stained with CD45, Live/Dead, Lineage, CD11b, MHCII, Ly6C, CD11c, XRC1, CD209b, Tim4, CD169, CD64, CD86, F4/80, MHCII, CD68, NK1.1, CD4 and CD8. Lymphocytes were initially gated on a forward scatter/side scatter by excluding the cells which displayed a size lower than 30k and were identified based on a linear relationship between FSC-H and FSC-A, followed by SSC-H and SSC-A. Leukocytes were defined as CD45+, and live leukocytes were selected based on low staining for Live/Dead Zombie UV. From this immune cells were selected as follows: T cells CD45+, TCRβ+/CD8+, B cells CD45+/TCRβ-/CD19+, NK cells CD45+/TCRβ-/CD19+/NK1.1+, neutrophils were selected as CD45+/TCRβ-/CD19-/Ly6G+/CD11b+, monocytes CD45+/TCRβ-/CD19-/Ly6G+/CD11b+/Ly6C+/lowMHCII, macrophages and DCs CD45+/TCRβ-/CD19-/Ly6G+/CD11b+/Ly6C+/MHCII+/CD11c+.